Hadamard Representations: Augmenting Hyperbolic Tangents in RL

Jacob E. Kooi
Department of Computer Science
Vrije Universiteit Amsterdam
Amsterdam, Netherlands.
j.e.kooi@vu.nl

Mark Hoogendoorn
Department of Computer Science
Vrije Universiteit Amsterdam
Amsterdam, Netherlands.
m.hoogendoorn@vu.nl

Vincent François-Lavet
Department of Computer Science
Vrije Universiteit Amsterdam
Amsterdam, Netherlands.
v.francoislavet@vu.nl

Abstract

Activation functions are one of the key components of a deep neural network. The most commonly used activation functions can be classed into the category of continuously differentiable (e.g. tanh) and linear-unit functions (e.g. ReLU), both having their own strengths and drawbacks with respect to downstream performance and representation capacity through learning (e.g. measured by the number of dead neurons and the effective rank). In reinforcement learning, the performance of continuously differentiable activations often falls short as compared to linear-unit functions. We provide insights into the vanishing gradients associated with the former, and show that the dying neuron problem is not exclusive to ReLU's. To alleviate vanishing gradients and the resulting dying neuron problem occurring with continuously differentiable activations, we propose a Hadamard representation. Using deep Q-networks and proximal policy optimization in the Atari domain, we show faster learning, a reduction in dead neurons and increased effective rank.

1 Introduction

Out of all activation functions, the Rectified Linear Unit (ReLU) [Fukushima, 1969, Nair and Hinton, 2010] and its variants [Xu et al., 2015, Klambauer et al., 2017] have emerged as the most widely used and generally best-performing activation functions up until this day [Jarrett et al., 2009, Goodfellow et al., 2016]. The strength of the ReLU activation lies in its ability to naturally avoid vanishing gradients when used in deeper networks, in contrast to the continuously differentiable activation functions, such as the sigmoid and the hyperbolic tangent [Glorot and Bengio, 2010].

A common drawback of using the ReLU activation is its limited expressivity in the context of

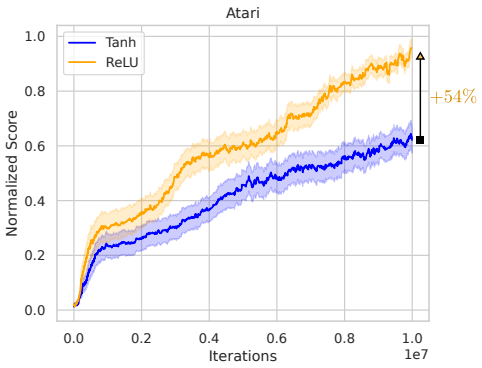

Figure 1: Normalized performance training DQN in the Atari domain where the nonlinear activation function of the representation, defined as the final hidden layer, is either ReLU or tanh. A strong performance discrepancy due to a relatively small architectural change can be observed.

17th European Workshop on Reinforcement Learning (ewrl 2024).

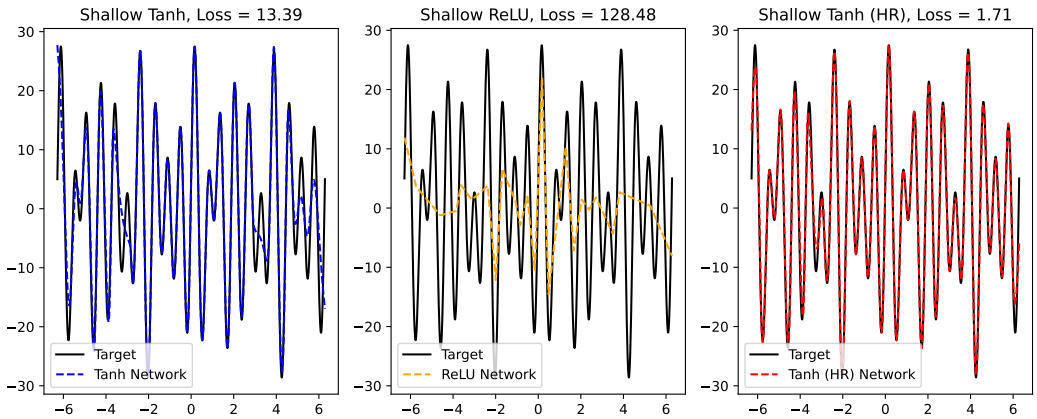

Figure 2: A regression of three shallow neural network architectures on a random complex sinusoidal function ($y = 10 * torch.sin(7 * x) + 15 * torch.sin(10 * x) + 5 * torch.cos(5 * x)$). The Tanh (HR) network emerges as the strongest function approximator, even while having less trainable parameters (501 vs 601 for Tanh & ReLU). To make a fair comparison, the Tanh and ReLU networks have one single hidden layer of size 200, while the Tanh (HR) network has a hidden layer of size 100. For the Tanh (HR) network however, we use two parallel linear layers preceding the hidden layer in order to be able to use the single hidden layer as the Hadamard product of two activations (see Section 3). For experiments comparing deeper networks, we refer the reader to Appendix C.1.

shallow networks (see Figure 2), as well as the phenomenon known as the dying ReLU problem [He et al., 2015, Lu et al., 2019]. As training progresses, the number of dying ReLU's tend to increase, resulting in a dying network and losing network capacity [Dubey et al., 2022].

In reinforcement learning (RL) [Sutton and Barto, 2018], even though training results in a large number of dying ReLU's [Gulcehre et al., 2022, Sokar et al., 2023], the ReLU function still remains the most popular activation for performance reasons [Henderson et al., 2018]. Similar to general deep learning [Teney et al., 2024], continuously differentiable activation functions such as the hyperbolic tangent are therefore not commonly used in RL (see Fig. 1). However, one might argue that their symmetrical, bounded shape and smooth gradient landscape has optimization advantages that the ReLU falls short of. Recent findings also indicate that a hidden layer activated by a hyperbolic tangent displays a high effective rank and thus a high layer expressivity [Kumar et al., 2021, Gulcehre et al., 2022]. Despite being a theoretically sound candidate, its lack of success in RL has not been thoroughly investigated.

We therefore aim to provide insights into the hyperbolic tangent's suboptimality, revealing that the vanishing gradient problem leads to dying neurons and under-utilization of the full network capacity. Based on these insights, we mitigate said effects by augmenting the original architecture. Specifically, we focus our research on the activations of the compressed representation of an encoder, defined as the final hidden layer, and provide an alternative to the conventional parameterization of this representation. Our contributions can be summarized as follows:

- We show that dying hyperbolic tangents are a phenomenon of a similar scale as the dying ReLU problem.
- A Hadamard representation (HR) is proposed, defining a latent representation as the Hadamard product of two separate, individually parameterized activation vectors.
- We empirically show that, without hyperparameter tuning or the use of auxiliary losses, a Hadamard representation yields significant performance gains over a standard hyperbolic tangent in the Atari domain, and reveal how it decreases dying neurons and increases the internal representations' effective rank.

2 Preliminaries

We consider an agent acting within its environment, where the environment is modeled as a discrete Markov Decision Process (MDP) defined as a tuple $(\mathcal{S}, \mathcal{A}, T, R, \gamma)$. $\mathcal{S}$ is the state space, $\mathcal{A}$ is the action space, $T : \mathcal{S} \times \mathcal{A} \to \mathcal{S}$ is the environment's transition function, $R : \mathcal{S} \times \mathcal{A} \to \mathcal{R}$ is the environment's reward function and $\gamma \in [0, 1)$ is the discount factor. A replay buffer B is used to store visited states $s_t \in \mathcal{S}$ that were followed by actions $a_t \in \mathcal{A}$ and resulted in the rewards $r_t \in \mathcal{R}$ and the next states s_{t+1}. One entry in B contains a tuple of past experience (s_t, a_t, r_t, s_{t+1}). The agent's goal is to learn a policy $\pi : \mathcal{S} \to \mathcal{A}$ that maximizes the expectation of the discounted return $V^\pi(s) = \mathbb{E}_\tau[\sum_{t=0}^{\infty} \gamma^t R(s_t, a_t) \mid s_t = s]$, where τ is a trajectory following the policy π.

Furthermore, we examine the setting where a high-dimensional state ($s_t \in \mathbb{R}^v$) is compressed into lower-dimensional activations $z_t \in \mathcal{Z} = \mathbb{R}^w$ where we call $\mathcal{Z}$ the representation space with $w \leq v$. This is done by means of a neural network encoding $e : \mathcal{S} \to \mathcal{Z}$ where e represents the encoder.

3 Augmenting Hyperbolic Tangents

Continuously differentiable activations such as the hyperbolic tangent ($tanh$) and the sigmoid (σ) activations are fundamentally different than the $ReLU$ or its Linear-Unit descendants, which are non-symmetric and have a large part of the input space mapped to zero (leading to sparsity). The hyperbolic tangent and the sigmoid output values in the ranges $[-1, 1]$ and $[0, 1]$, respectively. These functions are defined as:

$$tanh(x) = \frac{e^x - e^{-x}}{e^x + e^{-x}}, \qquad \sigma(x) = \frac{1}{1 + e^{-x}} \tag{1}$$

Both functions have the advantage of being differentiable everywhere, as well as being bounded. Furthermore, the sigmoid is well suited for output probabilities, while the tanh is convenient when requiring a zero-centered symmetrical output. However, both functions exhibit the vanishing gradient problem for saturating activations [Glorot and Bengio, 2010, Goodfellow et al., 2016].

Dying Hyperbolic Tangents

Although common literature has focused on the dying ReLU problem [He et al., 2015, Lu et al., 2019, Gulcehre et al., 2022, Sokar et al., 2023], we find that hidden layers activated by hyperbolic tangents similarly show strong dying neuron behavior. When using a hyperbolic tangent in a deep neural network, a single neuron $\alpha_i, i \in \mathbb{R}^w$, with w the layer dimension, can be classified as dying if:

$$|\alpha_i| \approx 1 \; \forall \; s_t \in B \tag{2}$$

Where s_t is an observation in buffer B. Note that an absolute value is used, as a hyperbolic tangent can either saturate towards -1 or 1. Given that the hyperbolic tangent is an asymptotic function near its saturation point, an approximate equality must be considered, as the classification of its saturation will always remain qualitative ($|\alpha_i| \neq 1 \; \forall \; s_t \in B$) . To approximate the condition given in Eq. 2, the amount of dying hyperbolic tangents is calculated by using a kernel density estimation (KDE) [Silverman, 1986] on the activations $\alpha_i, i \in \mathbb{R}^w$ of each individual neuron in the activation layer. In order to visualize activations in a hidden layer, a fixed subset of the KDE's of the neurons α_i is taken. A visualization of dying hyperbolic tangents in the Atari Breakout environment can be seen by analyzing sixteen individual neuron KDE's in Fig. 3.

More details on the KDE calculation and dying neuron classification can be found in Appendix B.

Hadamard Representations (HR)

As Fig. 3 indicates that the activation of z_t with a hyperbolic tangent leads to saturation and dying neurons, an augmentation of the representation architecture is proposed. In the conventional encoder setting, the networks' final hidden layer is defined as $z^{enc}(x) = f(A_1 x + B_1)$, with A_i and B_i representing weight and bias parameters, the function $f()$ representing a nonlinear activation function while x is the set of activations from the previous layer. In order to reduce the information dependence

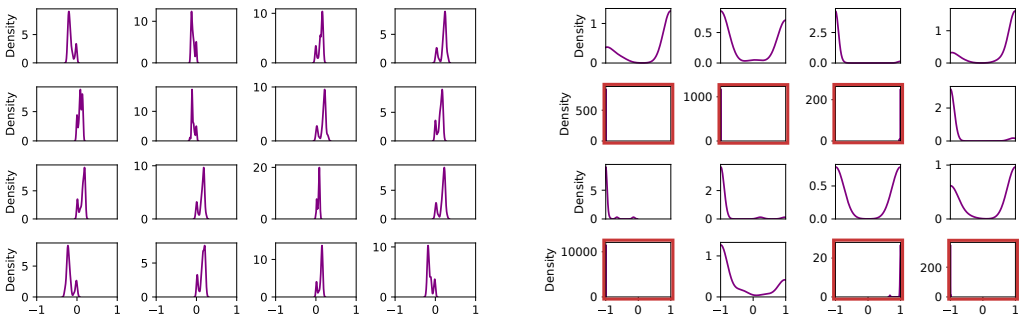

(a) Tanh - 10^6 iterations (b) Tanh - 10^7 iterations

Figure 3: Kernel Density Estimations (KDE) over a subset of 16 neurons in the compressed representation z_t after training DQN Mnih et al. [2015] in the Breakout environment using a hyperbolic tangent activation for z_t. Each neuron represents one dimension of the representation $z_t \in \mathbb{R}^{512}$. Red outlines represent dying neurons, where a near infinite sized density spike occurs at either 1 or -1.

on a single set of neurons, we propose using a Hadamard representation that augments the original representation with a parallel representation layer z^*. This can be interpreted as using a single highway layer with a closed carry gate [Srivastava et al., 2015]. The final representation is defined as the Hadamard product between the aforementioned activations $z(x) = z^{enc}(x) \cdot z^*(x)$, where $z^*(x) = f(A_2 x + B_2)$. A visualization of the proposed architecture can be found in Fig. 4.

Preventing Dying Neurons

Our key hypothesis is that the Hadamard representation can prevent saturation, hence alleviating vanishing gradients and dying neurons (See Eq. 2). To support our hypothesis, we investigate the derivative of a product of two functions. For the product of two arbitrary functions $g(x) \cdot h(x)$, the derivative is defined as $g'(x)h(x) + g(x)h'(x)$. In the context of using a sigmoid activation function for $f(x)$, the derivative of $z(x)$ becomes:

$$\begin{aligned} z'(x) = & A_1\sigma(A_1x + B_1)(1 - \sigma(A_1x + B_1))\sigma(A_2x + B_2) \\ & + A_2\sigma(A_1x + B_1)\sigma(A_2x + B_2)(1 - \sigma(A_2x + B_2)) \end{aligned}$$

If a neuron from $f(A_1x + B_1) = 0 \; \forall \; x$, the gradient of the product becomes 0 while if a positive saturation is experienced i.e. $f(A_1x + B_1) = 1 \; \forall \; x$, $z'(x)$ can remain nonzero. For a product of two hyperbolic tangent functions, the derivative is defined as:

$$h'(x) = A_1 \text{sech}^2(A_1x + B_1)\tanh(A_2x + B_2) + A_2 \text{sech}^2(A_2x + B_2)\tanh(A_1x + B_1)$$

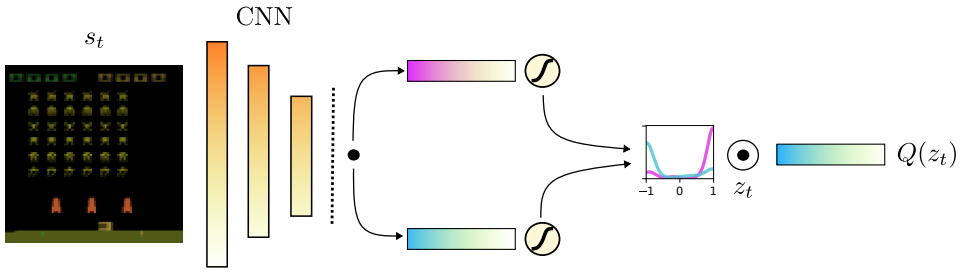

Figure 4: A visualisation of the Hadamard Representation architecture combined with the nature DQN architecture applied on a snapshot of the 'SpaceInvaders' Atari environment [Mnih et al., 2015]. Vertical and horizontal bars represent convolutional and linear layers, respectively. A parallel linear layer providing independently parameterized hidden layer activations is integrated, where the Hadamard product of the two activations represents the final latent representation z_t used for downstream learning.

where sech^2 is the derivative of a hyperbolic tangent. When using a hyperbolic tangent, the key difference with a sigmoid is that for any saturating value of $g(x)$, it will consistently keep the second part of the equation nonzero and dominated by $h(x)$, due to the hyperbolic tangents' saturation into strictly nonzero values. This means that during saturation of a neuron in $g(x)$, the non-saturated function $h(x)$ is still able to maintain a non-trivial gradient in the product derivative $h'(x)$, thus providing a mechanism to avoid vanishing gradients. We visualize the kernel densities during training in Fig. 5. The individual representations before taking the Hadamard product can be found in Appendix B.

Taking a more formal approximation of neuron collapse, we define the probability of a single neuron saturating as $\mathbf{p}$. Furthermore, in the case of a sigmoid or hyperbolic tangent, we assume symmetric saturation probabilities to both ends, defining the probability of a neuron saturating to one end of the spectrum as $0.5\mathbf{p}$. Under these assumptions, we show that interpreting a neuron as the product of two individual neurons will change saturation probabilities depending on the neuron activation function.

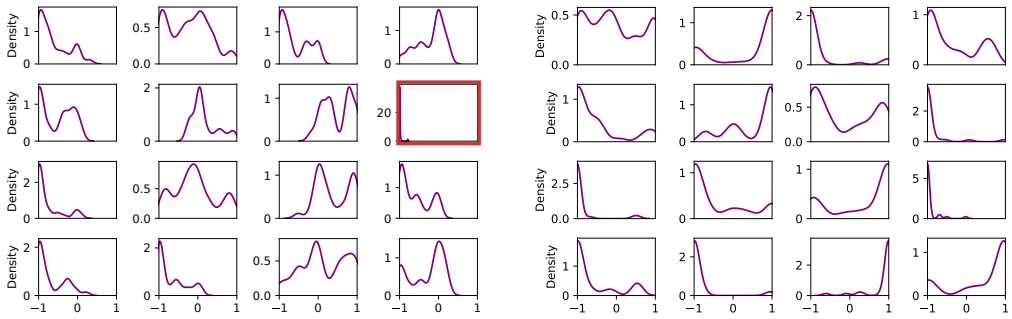

(a) Tanh (HR) - 10^6 iterations

(b) Tanh (HR) - 10^7 iterations

Figure 5: Kernel Density Estimations (KDE) over a subset of 16 neurons in the compressed representation z_t after training 'nature' DQN in the Breakout environment using a Hadamard representation (HR) with hyperbolic tangents. The Hadamard representation tends to more quickly utilize the full range of the hyperbolic tangent while also mitigating dying neurons.

Hyperbolic Tangent: In the case of the hyperbolic tangent, product saturation only occurs if strictly both neurons are saturated. This results in a probability of $\mathbf{p} \cdot \mathbf{p} = \mathbf{p}^2$. Taking a product of hyperbolic tangent activated neurons thus reduces the probability of neuron saturation from $\mathbf{p}$ to $\mathbf{p}^2$.

Table 1: Predicted dying neuron probabilities with and without a Hadamard representation.

Activation Function	**Dying Neuron Probability**	**Probability with HR**	**Difference**
Hyperbolic Tangent	$\mathbf{p}$	$\mathbf{p}^2$	$-(\mathbf{p}-\mathbf{p}^2)$
Sigmoid	$\mathbf{p}$	$\mathbf{p}$	0
ReLU	$\mathbf{p}$	$2\mathbf{p}-\mathbf{p}^2$	$+(\mathbf{p}-\mathbf{p}^2)$

Sigmoid: For the sigmoid function, product saturation occurs in two scenarios: Either one of the neurons is saturated towards zero or both neurons are saturated towards 1. The probability that a single neuron does not saturate towards zero is $(1-0.5\mathbf{p})$, and subsequently the probability that neither neuron saturates towards zero is $(1-0.5\mathbf{p})^2$. The probability that at least one of the two neurons saturates to zero is therefore $1-(1-0.5\mathbf{p})^2 = \mathbf{p}-0.25\mathbf{p}^2$. Adding the probability that both neurons saturate towards 1, which is $(0.5\mathbf{p})^2 = 0.25\mathbf{p}^2$, the final probability of the neuron product saturation is $\mathbf{p}-0.25\mathbf{p}^2+0.25\mathbf{p}^2 = \mathbf{p}$. Taking a product of sigmoid activated neurons therefore does not reduce the probability of neuron collapse.

Rectified Linear-Unit: In the case of a ReLU activation, we also assume the probability of a single neuron dying to be $\mathbf{p}$. As we look at the product of two neurons, the probability that one of the two neurons does not saturate is therefore $1-\mathbf{p}$, and the probability that both neurons do not saturate is

$(1-\mathbf{p})^2$. The probability that at least one neuron saturates is thus equal to $1-(1-\mathbf{p})^2 = 2\mathbf{p}-\mathbf{p}^2$. As the ReLU saturation results in strict zeroes, this results in the product also being zero. Taking a product of ReLU activated neurons therefore increases the final neuron saturation probability from $\mathbf{p}$ to $2\mathbf{p}-\mathbf{p}^2$. For an overview, we refer the reader to both Table 1 and the corresponding empirical evidence in Appendix C.3.

4 Experiments

The main experiments and discussion are conducted with the value-based DQN algorithm [Mnih et al., 2015] in Atari, and complemented by an evaluation on the policy-based proximal policy optimization algorithm (PPO) [Schulman et al., 2017]. In all experiments, we build on the strong baseline implementations from `cleanrl` [Huang et al., 2022]. For more details on the PPO and DQN implementation, we refer the reader to Appendix A.1. For both DQN and PPO, we define the representation $z_t \in \mathbb{R}^{512}$ as the last hidden layer of the network, which serves as the compressed representation of the original pixel observation s_t (see Fig. 4).

We perform all experiments on 8 common, non-exploration driven Atari games. We aim to show the effect of a Hadamard representation on the representations' fraction of dying neurons, its effective rank and its downstream performance. The dying neurons and the effective rank are calculated according to Appendix. B.1 and Appendix. B.2, respectively. The performance is aggregated over 8 environments and normalized using the ReLU baseline scores. Additionally, we show in Appendix D.1 that human-normalized scores tend to provide an even higher evaluation score for our algorithm.

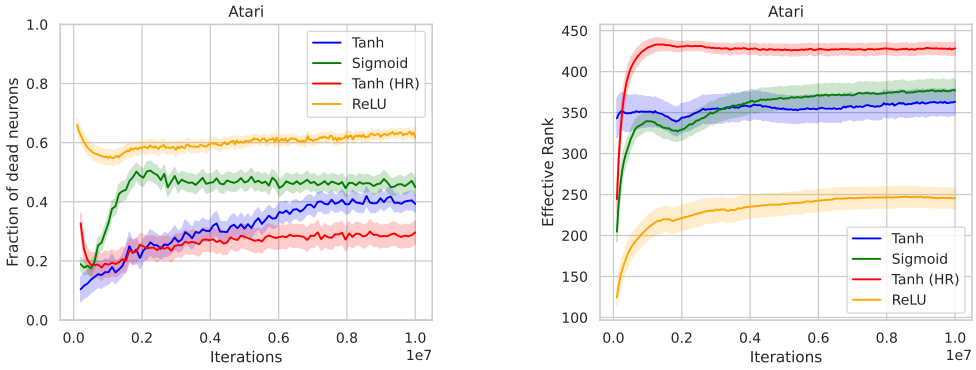

(a) Dead Neurons (b) Effective Rank

Figure 6: The average fraction of dead neurons (a) and the average effective rank [Kumar et al., 2021] (b) of the representation z_t when training DQN in the Atari domain for 10M iterations (40M frames). Similar to the well-known dying ReLU problem, hyperbolic tangent and sigmoid activations also exhibit strong dying neuron behavior during training. A Hadamard product of hyperbolic tangents reduces dead neurons in z_t and subsequently increases the effective rank of the representation.

Mitigating dying Hyperbolic Tangents

As mentioned in Section 3 and defined in Eq. 2, the number of dead neurons is equal to the amount of neurons that display the same saturated output for any given observation s_t. The amount of dead neurons over time when training on Atari can be seen in 6a. For the ReLU activation, around 60% of the neurons in the representation z_t end up dead, while for the sigmoid and hyperbolic tangent activation this number is around 40%. When using a hyperbolic tangent Hadamard representation, a reduction in dead neurons as compared to using a single hyperbolic tangent can be observed. We credit this to the inherent ability of a Hadamard product of hyperbolic tangents to minimize long-term activation saturation, as explained in Section 3. Quantitative results of dead neurons can be found in Table 2, which is correlated with earlier predictions from Table 1.

More corresponding dying neuron graphs for individual activations can be found in Appendix C.3. This reduction of long-term dead hyperbolic tangents when using an HR is remarkable as it is also

coinciding with a stronger divergence of values in the initial stages of training (see Fig. 5), which is usually a precursor to gradient saturation.

Increasing Effective Rank

We additionally calculate the effective rank [Kumar et al., 2021] of the representation z_t during training, which can be seen in Fig. 6b. As observed by Gulcehre et al. [2022], a representation activated by a hyperbolic tangent or a sigmoid, already has a relatively high effective rank compared to a representation activated by a ReLU. Furthermore, as can additionally be seen in supervised learning (see Fig. 2), using a Hadamard representation notably improves the effective rank, which can be seen as a measure of network 'expressivity'.

Analyzing Performance in Atari

The influence of a Hadamard representation on downstream performance can be seen in Fig. 7. A significant improvement of nearly 60% over the standard hyperbolic tangent baseline is obtained, as well as an improvement over the default ReLU baseline. Note that no hyperparameter or architectural tuning has been employed in these experiments.

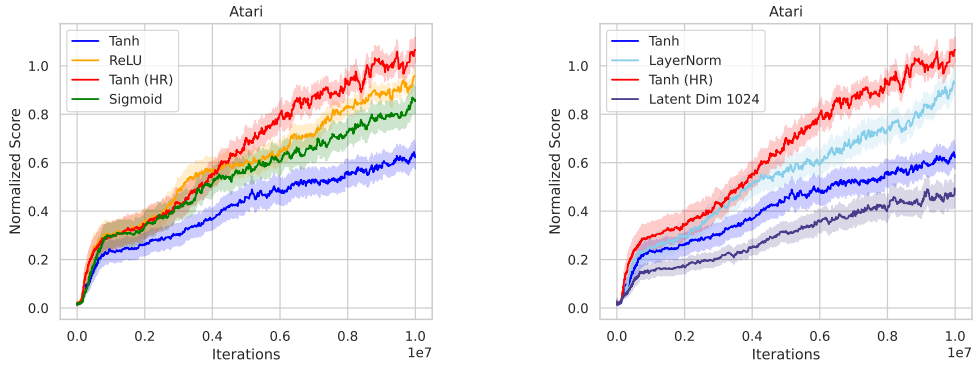

(a) Normalized Score (b) Ablations

Figure 7: Normalized performance with the standard deviation over the means in the Atari domain, after training DQN for 10M iterations (40M Frames). In (a), the Tanh (HR) stronly outperforms a the baseline Tanh. In (b), several ablations including layer normalization [Ba et al., 2016] on hyperbolic tangent activations are shown. Notably, the decrease in performance when using a conventional representation with twice as much neurons ($z_t \in \mathbb{R}^{1024}$) shows that more parameters are not always desirable. Additional experiments combining the ReLU activation with a Hadamard representation can be found in Appendix C.4.

Examining further ablations in Fig. 8 shows that using a sophisticated Linear-Unit function such as the SELU activation [Klambauer et al., 2017] or using an addition rather than a product of hyperbolic tangents seems detrimental to performance. Furthermore, taking a product of 3 hyperbolic tangents (2HR) also appears to enhance performance, though there seems to be a negative effect in the early stages of training as compared to using a single Hadamard product. We hypothesize that this is the result of increased contracting behavior in the early stage of training due to increasing multiplication of hyperbolic tangent activations whose absolute values are < 1.

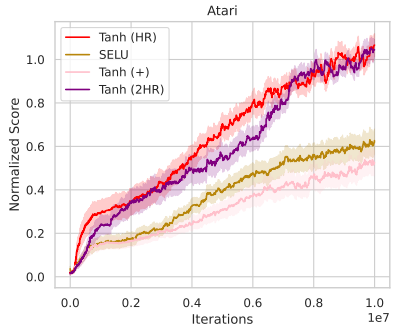

Figure 8: Additional ablations run on DQN in the Atari domain. Tanh (+) represents an addition rather than a Hadamard product, and Tanh (2HR) uses a triple Hadamard product.

Table 2: Dying neuron fractions with and without a Hadamard representation (HR).

Activation Function	Dead Neuron Fraction	Dead Neuron Fraction (HR)	Difference
Hyperbolic Tangent	0.39	0.30	-23%
Sigmoid	0.44	0.45	+2%
ReLU	0.62	0.73	+18%

Evaluating Hadamard representations on PPO

To evaluate results on a policy-based algorithm, additional experiments are run using the PPO algorithm [Schulman et al., 2017]. For PPO, the internal architectural difference with DQN is that the compressed representation z_t precedes both a critic and an actor network, and thus receives policy and value gradients (see Appendix A.2). The results can be found in Fig. 9. Similarly to the results on DQN, the Tanh (HR) exhibits the highest effective rank and the best performance. The Tanh (HR) and the ReLU also seem to have consistent strong performance across both algorithms, whereas the pure hyperbolic tangent and sigmoid activations seem relatively unreliable across algorithms.

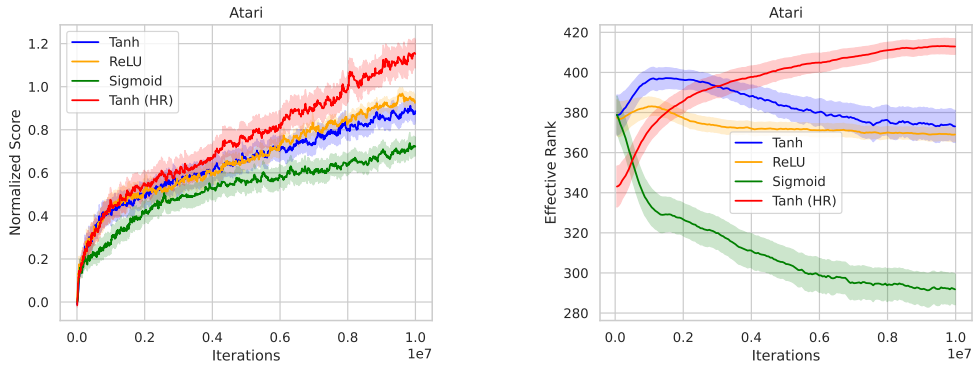

(a) Normalized Score (b) Effective Rank

Figure 9: Normalized performance (a) and effective rank (b) in the Atari domain for 10M iterations (40M Frames) when training the PPO algorithm [Schulman et al., 2017].

Interestingly, it seems that the ReLU activations' performance is less correlated to its low effective rank and high amount of dying neurons than the continuously differentiable activations. As also indicated by Teney et al. [2024], the exact reasons for the broad success of the ReLU activations are not yet fully understood. A qualitative overview of our results can be found in Table 3.

Table 3: High-level summary of the strengths of a Hadamard representation.

Activation function	Performance RL	Few dead neurons	Effective rank
Tanh (HR)	++	++	++
Tanh	-	-	+
ReLU	+	--	--
Sigmoid	-	-	-

Increasing Representation Dimensionality

A Hadamard representation increases the amount of trainable parameters in the encoder without increasing the dimension of the representation $z_t \in \mathbb{R}^{512}$. This is an important feature as simply increasing the dimension of the representation to $\mathbb{R}^{1024}$ is not often effective (see Fig. 7b). Even though the fraction of dying ReLU's decreases and the effective rank increases when using $z_t \in \mathbb{R}^{1024}$,

it seems that the 'relative' effective rank, defined as the ratio $\frac{rank}{dim(z_t)}$, actually goes down (See Appendix. C.2). We therefore hypothesize that trying to reduce dying neurons and to increase a representations' effective rank is only superficially solved by increasing representation dimensionality.

5 Related Work

Network Capacity in RL. Liu et al. [2019] investigated the need for sparse representations in the continuous control domain. Gulcehre et al. [2022] analyzed network expressiveness in RL by measuring the effective rank [Kumar et al., 2021] of the compressed representation, and found that hyperbolic tangent representations generally maintain high rank and do not suffer strongly from rank decay as training continues. Related work used normalization techniques and action penalization to counteract high variance in pixel-based robotic control [Bjorck et al., 2022]. Other work by Lyle et al. [2022] investigated capacity loss in RL and similarly found that, as training progresses, the inherent network capacity of RL algorithms decays. Further research by Nikishin et al. [2022] used network resets to counteract the primacy bias and Sokar et al. [2023] evaluated and mitigated the dying ReLU phenomenon in DQN, both operating in the sample efficiency setting. Nikishin et al. [2023] further studied plasticity injection for long-term training. In another related direction, recent work has investigated network sparsity in RL, showing that a large part of network capacity might be unnecessary when training reinforcement learning [Arnob et al., 2021, Graesser et al., 2022, Sokar et al., 2022, Tan et al., 2023, Obando-Ceron et al., 2024]. This provides further insights into why a ReLU can achieve strong performance despite resulting in a significant number of dead neurons.

Network Architecture in RL The origin of network optimization problems with hyperbolic tangents and sigmoids were empirically investigated by Glorot and Bengio [2010], where, according to the authors, a lot of mystery still surrounds the subject. Work by Srivastava et al. [2015] in supervised learning first looked at the idea of using products of hidden layers together with a 'gate' that determined the amount of information flow [Hochreiter and Schmidhuber, 1997]. Using these ideas, the Resnet was invented [He et al., 2016] and also showed strong performance in combination with RL [Espeholt et al., 2018]. Further work by Henderson et al. [2018] showed differences in RL performances over different network architectures and nonlinear activations. Work by Abbas et al. [2023] successfully applied ReLU concatenation [Shang et al., 2016] to improve continual learning while keeping a similar performance when training from scratch. Finally, recent work by Grooten et al. [2024] investigated raw pixel masking for distractions in RL using a parallel CNN input layer.

6 Conclusions and Discussion

This paper analyzed issues with continuously differentiable activations in RL and demonstrated that these activation functions also suffer from the dying neuron problem. In response, we propose a novel representation architecture, the Hadamard Representation (HR), which enhances an encoder's final hidden layer by taking the Hadamard product with a parallel, independently parameterized activation layer. We further discussed and empirically showed that applying the Hadamard representation with hyperbolic tangents reduces the occurrence of dead neurons in the representation and increases layer expressiveness. Notably, this approach significantly improved performance in Atari games compared to both standard representation parameterizations and merely increasing the representation dimension.

As investigated by Kumar et al. [2021], a compressed representation activated by a hyperbolic tangent attains a much higher effective rank than when activated by a ReLU, and will therefore yield stronger network expressiveness. In light of this, the hyperbolic tangent can potentially replace the ReLU in a variety of architectures where expressiveness is required without using deeper networks.

Future work could focus on further identifying the intricacies of hyperbolic tangents in an attempt to push the potential of continuously differentiable activations in reinforcement learning or even in a supervised learning setting (see Fig. 2). Also, we believe that an implementation of Hadamard-style architectures in a continual learning setting with similar evaluations as in Abbas et al. [2023] could be promising.

7 Limitations

Our work has focused on the encoders' final hidden layer in reinforcement learning. Both preliminary experiments and literature suggest that convolutional layers have a very strong preference for rectified activations [Jarrett et al., 2009], possibly due to a low-frequency bias [Ramasinghe and Lucey, 2022, Teney et al., 2024]. We have therefore not conducted experiments integrating Hadamard representations in the convolutional section of our encoder architectures. A hyperparameter search could further strengthen our results, since the baseline is specifically tuned for the ReLU activation. Furthermore, as we perform experiments on DQN and PPO, integration of a Hadamard representation into more sophisticated algorithms and architectures such as Rainbow [Hessel et al., 2018] and Impala [Espeholt et al., 2018] would be interesting.

References

Zaheer Abbas, Rosie Zhao, Joseph Modayil, Adam White, and Marlos C. Machado. Loss of plasticity in continual deep reinforcement learning. In Sarath Chandar, Razvan Pascanu, Hanie Sedghi, and Doina Precup, editors, *Proceedings of The 2nd Conference on Lifelong Learning Agents*, volume 232 of *Proceedings of Machine Learning Research*, pages 620–636. PMLR, 22–25 Aug 2023. URL https://proceedings.mlr.press/v232/abbas23a.html.

Samin Yeasar Arnob, Riyasat Ohib, Sergey M. Plis, and Doina Precup. Single-shot pruning for offline reinforcement learning. *CoRR*, abs/2112.15579, 2021. URL https://arxiv.org/abs/2112.15579.

Jimmy Lei Ba, Jamie Ryan Kiros, and Geoffrey E. Hinton. Layer normalization, 2016. URL http://arxiv.org/abs/1607.06450. cite arxiv:1607.06450.

Johan Bjorck, Carla P Gomes, and Kilian Q Weinberger. Is high variance unavoidable in RL? a case study in continuous control. In *International Conference on Learning Representations*, 2022. URL https://openreview.net/forum?id=9xhgmsNVHu.

Shiv Ram Dubey, Satish Kumar Singh, and Bidyut Baran Chaudhuri. Activation functions in deep learning: A comprehensive survey and benchmark. *Neurocomputing*, 503:92–108, 2022. ISSN 0925-2312. doi: https://doi.org/10.1016/j.neucom.2022.06.111. URL https://www.sciencedirect.com/science/article/pii/S0925231222008426.

Lasse Espeholt, Hubert Soyer, Remi Munos, Karen Simonyan, Vlad Mnih, Tom Ward, Yotam Doron, Vlad Firoiu, Tim Harley, Iain Dunning, Shane Legg, and Koray Kavukcuoglu. IMPALA: Scalable distributed deep-RL with importance weighted actor-learner architectures. In Jennifer Dy and Andreas Krause, editors, *Proceedings of the 35th International Conference on Machine Learning*, volume 80 of *Proceedings of Machine Learning Research*, pages 1407–1416. PMLR, 10–15 Jul 2018. URL https://proceedings.mlr.press/v80/espeholt18a.html.

Kunihiko Fukushima. Visual feature extraction by a multilayered network of analog threshold elements. *IEEE Transactions on Systems Science and Cybernetics*, 5(4):322–333, 1969. doi: 10.1109/TSSC.1969.300225.

Xavier Glorot and Yoshua Bengio. Understanding the difficulty of training deep feedforward neural networks. In Yee Whye Teh and Mike Titterington, editors, *Proceedings of the Thirteenth International Conference on Artificial Intelligence and Statistics*, volume 9 of *Proceedings of Machine Learning Research*, pages 249–256, Chia Laguna Resort, Sardinia, Italy, 13–15 May 2010. PMLR. URL https://proceedings.mlr.press/v9/glorot10a.html.

I. Goodfellow, Y. Bengio, and A. Courville. *Deep Learning*. Adaptive computation and machine learning. MIT Press, 2016. ISBN 9780262035613. URL https://books.google.co.in/books?id=Np9SDQAAQBAJ.

Laura Graesser, Utku Evci, Erich Elsen, and Pablo Samuel Castro. The state of sparse training in deep reinforcement learning. In Kamalika Chaudhuri, Stefanie Jegelka, Le Song, Csaba Szepesvari, Gang Niu, and Sivan Sabato, editors, *Proceedings of the 39th International Conference on Machine Learning*, volume 162 of *Proceedings of Machine Learning Research*, pages 7766–7792. PMLR, 17–23 Jul 2022. URL https://proceedings.mlr.press/v162/graesser22a.html.

Bram Grooten, Tristan Tomilin, Gautham Vasan, Matthew E. Taylor, A. Rupam Mahmood, Meng Fang, Mykola Pechenizkiy, and Decebal Constantin Mocanu. Madi: Learning to mask distractions for generalization in visual deep reinforcement learning. In *International Conference on Autonomous Agents and Multiagent Systems, AAMAS*, 2024.

Caglar Gulcehre, Srivatsan Srinivasan, Jakub Sygnowski, Georg Ostrovski, Mehrdad Farajtabar, Matthew Hoffman, Razvan Pascanu, and Arnaud Doucet. An empirical study of implicit regularization in deep offline RL. *Transactions on Machine Learning Research*, 2022. ISSN 2835-8856. URL https://openreview.net/forum?id=HFfJWx60IT.

Kaiming He, Xiangyu Zhang, Shaoqing Ren, and Jian Sun. Delving deep into rectifiers: Surpassing human-level performance on imagenet classification. In *Proceedings of the IEEE international conference on computer vision*, pages 1026–1034, 2015.

Kaiming He, Xiangyu Zhang, Shaoqing Ren, and Jian Sun. Deep Residual Learning for Image Recognition. In *Proceedings of 2016 IEEE Conference on Computer Vision and Pattern Recognition*, CVPR '16, pages 770–778. IEEE, June 2016. doi: 10.1109/CVPR.2016.90. URL http://ieeexplore.ieee.org/document/7780459.

Peter Henderson, Riashat Islam, Philip Bachman, Joelle Pineau, Doina Precup, and David Meger. Deep reinforcement learning that matters. In *Proceedings of the Thirty-Second AAAI Conference on Artificial Intelligence and Thirtieth Innovative Applications of Artificial Intelligence Conference and Eighth AAAI Symposium on Educational Advances in Artificial Intelligence*, AAAI'18/IAAI'18/EAAI'18. AAAI Press, 2018. ISBN 978-1-57735-800-8.

Matteo Hessel, Joseph Modayil, Hado van Hasselt, Tom Schaul, Georg Ostrovski, Will Dabney, Dan Horgan, Bilal Piot, Mohammad Gheshlaghi Azar, and David Silver. Rainbow: Combining improvements in deep reinforcement learning. In Sheila A. McIlraith and Kilian Q. Weinberger, editors, *AAAI*, pages 3215–3222. AAAI Press, 2018. URL http://dblp.uni-trier.de/db/conf/aaai/aaai2018.html#HesselMHSODHPAS18.

Sepp Hochreiter and Jürgen Schmidhuber. Long short-term memory. *Neural Computation*, 9(8):1735–1780, 1997. doi: 10.1162/neco.1997.9.8.1735.

Shengyi Huang, Rousslan Fernand Julien Dossa, Chang Ye, Jeff Braga, Dipam Chakraborty, Kinal Mehta, and João G.M. Araújo. Cleanrl: High-quality single-file implementations of deep reinforcement learning algorithms. *Journal of Machine Learning Research*, 23(274):1–18, 2022. URL http://jmlr.org/papers/v23/21-1342.html.

Kevin Jarrett, Koray Kavukcuoglu, Marc'Aurelio Ranzato, and Yann LeCun. What is the best multi-stage architecture for object recognition? In *2009 IEEE 12th International Conference on Computer Vision*, pages 2146–2153, 2009. doi: 10.1109/ICCV.2009.5459469.

Günter Klambauer, Thomas Unterthiner, Andreas Mayr, and Sepp Hochreiter. Self-normalizing neural networks. In *Advances in Neural Information Processing Systems 30: Annual Conference on Neural Information Processing Systems 2017, December 4-9, 2017, Long Beach, CA, USA*, pages 971–980, 2017. URL https://proceedings.neurips.cc/paper/2017/hash/5d44ee6f2c3f71b73125876103c8f6c4-Abstract.html.

Aviral Kumar, Rishabh Agarwal, Dibya Ghosh, and Sergey Levine. Implicit under-parameterization inhibits data-efficient deep reinforcement learning. In *International Conference on Learning Representations*, 2021.

Vincent Liu, Raksha Kumaraswamy, Lei Le, and Martha White. The utility of sparse representations for control in reinforcement learning. In *Proceedings of the Thirty-Third AAAI Conference on Artificial Intelligence and Thirty-First Innovative Applications of Artificial Intelligence Conference and Ninth AAAI Symposium on Educational Advances in Artificial Intelligence*, AAAI'19/IAAI'19/EAAI'19. AAAI Press, 2019. ISBN 978-1-57735-809-1. doi: 10.1609/aaai.v33i01.33014384. URL https://doi.org/10.1609/aaai.v33i01.33014384.

Lu Lu, Yeonjong Shin, Yanhui Su, and George E. Karniadakis. Dying relu and initialization: Theory and numerical examples. *CoRR*, abs/1903.06733, 2019. URL http://dblp.uni-trier.de/db/journals/corr/corr1903.html#abs-1903-06733.

Clare Lyle, Mark Rowland, and Will Dabney. Understanding and preventing capacity loss in reinforcement learning. In *International Conference on Learning Representations*, 2022. URL https://openreview.net/forum?id=ZkC8wKoLbQ7.

Volodymyr Mnih, Koray Kavukcuoglu, David Silver, et al. Human-level control through deep reinforcement learning. *Nature*, 518(7540):529–533, 2 2015. doi: 10.1038/nature14236.

Vinod Nair and Geoffrey E Hinton. Rectified linear units improve restricted boltzmann machines. In *ICML 2010*, pages 807–814, 2010.

Evgenii Nikishin, Max Schwarzer, Pierluca D'Oro, Pierre-Luc Bacon, and Aaron Courville. The primacy bias in deep reinforcement learning. In Kamalika Chaudhuri, Stefanie Jegelka, Le Song, Csaba Szepesvari, Gang Niu, and Sivan Sabato, editors, *Proceedings of the 39th International Conference on Machine Learning*, volume 162 of *Proceedings of Machine Learning Research*, pages 16828–16847. PMLR, 17–23 Jul 2022.

Evgenii Nikishin, Junhyuk Oh, Georg Ostrovski, Clare Lyle, Razvan Pascanu, Will Dabney, and Andre Barreto. Deep reinforcement learning with plasticity injection. In A. Oh, T. Naumann, A. Globerson, K. Saenko, M. Hardt, and S. Levine, editors, *Advances in Neural Information Processing Systems*, volume 36, pages 37142–37159. Curran Associates, Inc., 2023. URL https://proceedings.neurips.cc/paper_files/paper/2023/file/75101364dc3aa7772d27528ea504472b-Paper-Conference.pdf.

Johan Obando-Ceron, Aaron Courville, and Pablo Samuel Castro. In deep reinforcement learning, a pruned network is a good network. *arXiv preprint arXiv:2402.12479*, 2024.

Sameera Ramasinghe and Simon Lucey. Beyond periodicity: Towards a unifying framework for activations in coordinate-mlps. In *European Conference on Computer Vision*, pages 142–158. Springer, 2022.

John Schulman, Filip Wolski, Prafulla Dhariwal, Alec Radford, and Oleg Klimov. Proximal policy optimization algorithms. *ArXiv*, abs/1707.06347, 2017. URL https://api.semanticscholar.org/CorpusID:28695052.

Wenling Shang, Kihyuk Sohn, Diogo Almeida, and Honglak Lee. Understanding and improving convolutional neural networks via concatenated rectified linear units. In Maria Florina Balcan and Kilian Q. Weinberger, editors, *Proceedings of The 33rd International Conference on Machine Learning*, volume 48 of *Proceedings of Machine Learning Research*, pages 2217–2225, New York, New York, USA, 20–22 Jun 2016. PMLR. URL https://proceedings.mlr.press/v48/shang16.html.

Bernard W Silverman. *Density Estimation for Statistics and Data Analysis*. Chapman and Hall, 1986.

Ghada Sokar, Elena Mocanu, Decebal Constantin Mocanu, Mykola Pechenizkiy, and Peter Stone. Dynamic sparse training for deep reinforcement learning. In Lud De Raedt, editor, *Proceedings of the Thirty-First International Joint Conference on Artificial Intelligence, IJCAI-22*, pages 3437–3443. International Joint Conferences on Artificial Intelligence Organization, 7 2022. doi: 10.24963/ijcai.2022/477. URL https://doi.org/10.24963/ijcai.2022/477. Main Track.

Ghada Sokar, Rishabh Agarwal, Pablo Samuel Castro, and Utku Evci. The dormant neuron phenomenon in deep reinforcement learning. In *Proceedings of the 40th International Conference on Machine Learning*, ICML'23. JMLR.org, 2023.

Rupesh K Srivastava, Klaus Greff, and Jürgen Schmidhuber. Training very deep networks. In C. Cortes, N. Lawrence, D. Lee, M. Sugiyama, and R. Garnett, editors, *Advances in Neural Information Processing Systems*, volume 28. Curran Associates, Inc., 2015. URL https://proceedings.neurips.cc/paper_files/paper/2015/file/215a71a12769b056c3c32e7299f1c5ed-Paper.pdf.

Richard S. Sutton and Andrew G. Barto. *Reinforcement Learning: An Introduction*. The MIT Press, second edition, 2018. URL http://incompleteideas.net/book/the-book-2nd.html.

Yiqin Tan, Pihe Hu, Ling Pan, Jiatai Huang, and Longbo Huang. Rlx2: Training a sparse deep reinforcement learning model from scratch. *CoRR*, abs/2205.15043, 2023. URL https://arxiv.org/abs/2205.15043.

Damien Teney, Armand Mihai Nicolicioiu, Valentin Hartmann, and Ehsan Abbasnejad. Neural redshift: Random networks are not random functions. In *Proceedings of the IEEE/CVF Conference on Computer Vision and Pattern Recognition (CVPR)*, pages 4786–4796, June 2024.

Bing Xu, Naiyan Wang, Tianqi Chen, and Mu Li. Empirical evaluation of rectified activations in convolutional network. *CoRR*, abs/1505.00853, 2015. URL http://arxiv.org/abs/1505.00853.

A Implementation Details

A.1 Hyperparameters

To evaluate, 8 different Atari environments are tested, using 5 different random seeds. For the mean scores, we take the mean over the eight environments. Our normalized score is calculated according to our baseline, the original implementation using a ReLU activation.

All the hyperparameters used in our experiments for DQN and PPO, respectively, are as reported in `cleanrl` [Huang et al., 2022]. The hyperparameters can be found in Table 1 and Table 2.

Table 4: DQN Hyperparameters

Hyperparameter	**Value**	**Description**
Learning Rate	1×10^{-4}	Learning rate for the optimizer
Discount Factor (γ)	0.99	Discount for future rewards
Replay Memory Size	1,000,000	Size of the experience replay buffer
Mini-batch Size	32	Number of samples per batch update
Target Network Update Frequency	1000	Update frequency for the target network
Initial Exploration	1.0	Initial exploration rate in ϵ-greedy
Final Exploration	0.1	Final exploration rate in ϵ-greedy
Final Exploration Frame	1,000,000	Frame number to reach final exploration
Exploration Decay Frame	1,000,000	Frames over which exploration rate decays
Action Repeat (Frame Skip)	4	Number of frames skipped per action
Reward Clipping	[-1, 1]	Range to which rewards are clipped
Input Dimension	84 x 84	Dimensions of the input image
Latent Dimension	512	Dimension of the latent representation
Input Frames	4	Number of frames used as input
Training Start Frame	80,000	Frame number to start training
Loss Function	Mean Squared Error	Loss function used for updates
Optimizer	Adam	Optimization algorithm used
Optimizer ϵ	10^{-5}	Adam Epsilon

Table 5: PPO Hyperparameters

Hyperparameter	**Value**	**Description**
Learning Rate	2.5×10^{-4}	Learning rate for the optimizer
Discount Factor (γ)	0.99	Discount factor for future rewards
Number of Steps	128	Number of steps per environment before update
Anneal LR	True	Whether to anneal the learning rate
GAE Lambda	0.95	Lambda parameter for GAE
Number of Minibatches	4	Number of minibatches to split the data
Update Epochs	4	Number of epochs per update
Normalize Advantage	True	Whether to normalize advantage estimates
Clipping Coefficient	0.1	Clipping parameter for PPO
Clip Value Loss	True	Whether to clip value loss
Entropy Coefficient	0.01	Coefficient for entropy bonus
Value Function Coefficient	0.5	Coefficient for value function loss
Maximum Gradient Norm	0.5	Maximum norm for gradient clipping
Target KL	None	Target KL divergence between updates
Latent Dimension	512	Dimension of the latent representation
Optimizer	Adam	Optimization algorithm used
Optimizer ϵ	10^{-5}	Adam Epsilon

Reinforcement Learning

In DQN, the action a_t is chosen following an ϵ-greedy policy. With probability ϵ, a random action is selected, and with $(1-\epsilon)$, the action maximizing the Q-value is chosen. The target Y_t is defined as:

$$Y_t = r_t + \gamma Q'(z_{t+1}, \arg\max_{a \in \mathcal{A}} Q(z_{t+1}, a)), \tag{3}$$

where $Q'(z, a)$ denotes the target Q-network, an auxiliary network that stabilizes the learning by providing a stable target for $Q(z, a)$. The parameters of Q' are updated less frequently to enhance learning stability. The loss function for training the network is:

$$\mathcal{L}_Q = \left|Y_t - Q(z_t, a)\right|^2. \tag{4}$$

Proximal Policy Optimization (PPO) operates on a different principle, utilizing policy gradient methods for policy improvement. PPO seeks to update the policy by maximizing an objective function while preventing large deviations from the previous policy through a clipping mechanism in the objective's estimator. The clipped policy gradient loss L^{CLIP} is defined as:

$$L^{CLIP}(\theta) = \mathbb{E}\left[\min(r_t(\theta)\hat{A}_t, \text{clip}(r_t(\theta), 1-\epsilon, 1+\epsilon)\hat{A}_t)\right], \tag{5}$$

where $r_t(\theta)$ represents the ratio of the probabilities under the new policy versus the old policy, and $\hat{A}_t$ is the advantage estimate at timestep t. This clipped surrogate objective ensures gradual and stable policy updates.

A.2 PPO Architecture

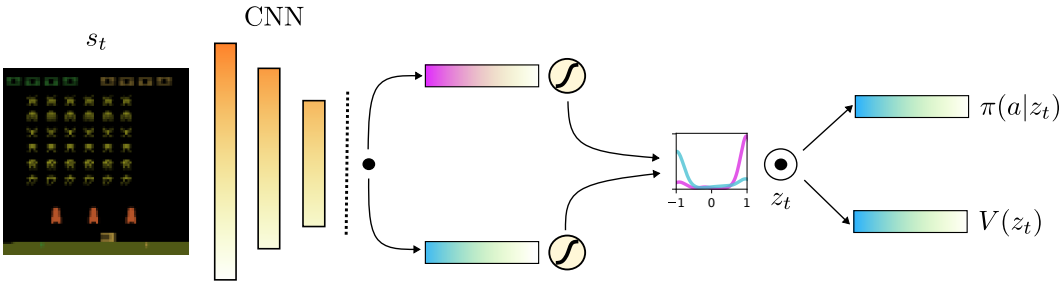

Figure 10: A visualisation of the Hadamard representation (HR) architecture combined with the PPO architecture applied on a snapshot of the 'SpaceInvaders' Atari environment. A parallel linear layer providing an independent representation is integrated, where the Hadamard product of the two parallel representations represents the final representation z_t.

B Kernel Density Estimations

As discussed in Section 3, we hypothesize that the differences between a hyperbolic tangent with and without an HR are due to the increased ability of the product of hyperbolic tangents being able to negate dying neurons. We further see this phenomenom when plotting a random selection of neurons from both the mask and the base representation in Fig. 11a.

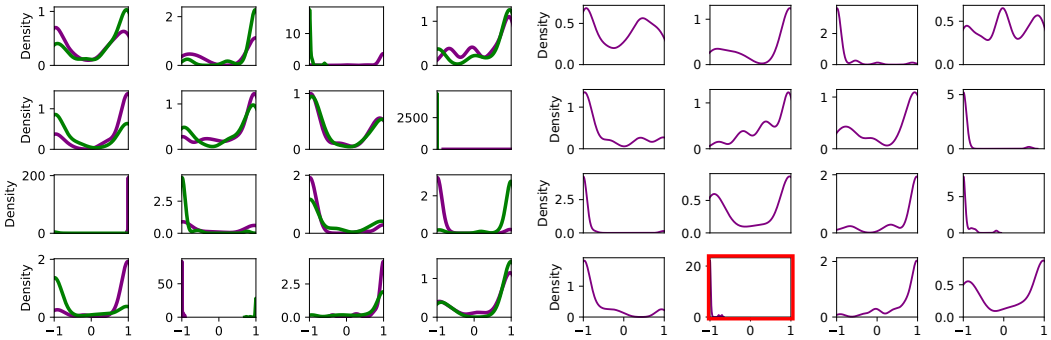

(a) Tanh (HR) - $5 \cdot 10^6$ iterations

(b) Final Tanh (HR) - $5 \cdot 10^6$ iterations

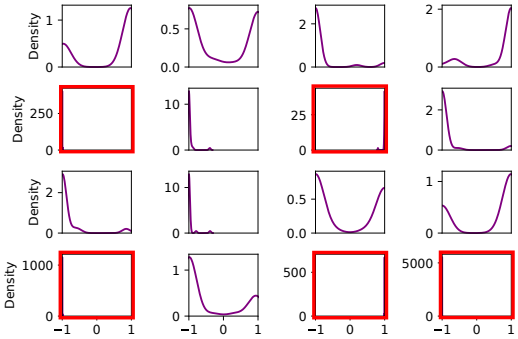

(c) Tanh (no HR) - $5 \cdot 10^6$ iterations

Figure 11: Kernel Density Estimations (KDE) over a subset of 16 neurons in the representations z_t^{enc} and z_t^* in (a), the resulting Hadamard product z_t in (b) and the representation z_t when training without an HR (c). These representations are obtained after training DQN in the 'Breakout' environment. Red outlines represent dead (collapsed) neurons. In (a), a closer look at neurons 3, 8 and 9 shows that when one of the representations saturates, the other is able to compensate, leading to a non-dead neuron in their product z_t in (b).

B.1 KDE calculation

Firstly, to stabilize the KDE computation and avoid singularity issues, a small noise ϵ, following a normal distribution, is added to each neuron's activations:

$$\alpha_i' = \alpha_i + \epsilon, \quad \epsilon \sim \mathcal{N}(0, \sigma^2)$$

where $\sigma^2 = 1 \times 10^{-5}$. The bandwidth for KDE, crucial for the accuracy of the density estimate, is calculated using Scott's rule, adjusted by the standard deviation of the jittered activations:

$$bw = n^{-\frac{1}{5}} \cdot \text{std}(\alpha_i')$$

where n is the number of samples in α_i. The density of activations is then estimated using a Gaussian kernel:

$$f(x) = \frac{1}{n \cdot bw} \sum_{j=1}^{n} K\left(\frac{x - \alpha_{ij}'}{bw}\right)$$

Here, K denotes the Gaussian kernel function. In order to finally determine if a neuron is dead, the maximum value of the estimated density function $f(x)$ is compared against a predefined threshold:

$$\max(f(x)) \geq \omega$$

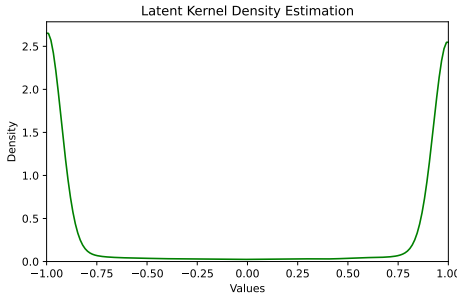

(a) Tanh - 10^7 iterations

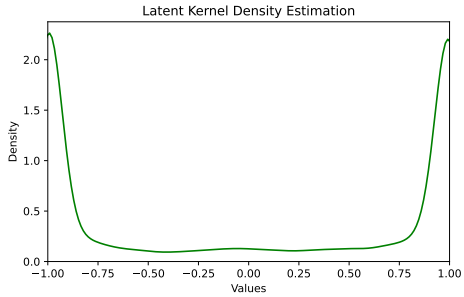

(b) Tanh (HR) - 10^7 iterations

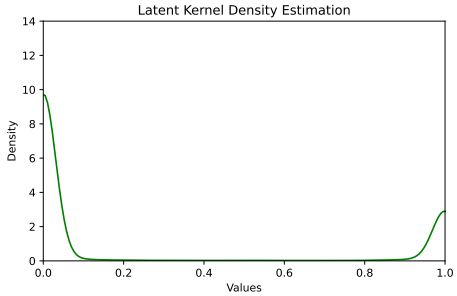

(c) Sigmoid - 10^7 iterations

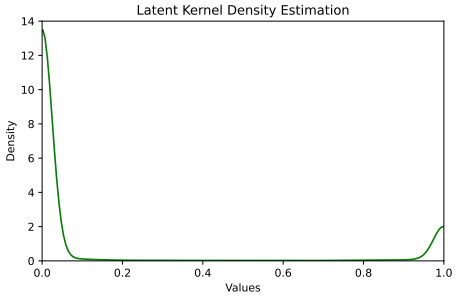

(d) Sigmoid (HR) - 10^7 iterations

Figure 12: Kernel Density Estimations of the final representation z_t after training DQN for 10^7 iterations in the Breakout environment. A hyperbolic tangent Hadamard representation allows the representation to avoid strong saturation, keeping sufficient kernel density in the central sections of the hyperbolic tangent. As a sigmoid can saturate into zero, using a Hadamard representation remains less effective into preventing saturation.

where ω represents the predetermined threshold. In practice, after analyzing the individual neuron KDE's, using an ω of 20 provides a strong approximation of actual dead neurons.

B.2 Effective Rank calculation

In line with Kumar et al. [2021], the effective rank of a feature matrix for a threshold δ ($\delta = 0.01$), denoted as $srank_\delta(\Phi)$, is given by $srank_\delta(\Phi) = \min\left\{k : \frac{\sum_{i=1}^{k}\sigma_i(\Phi)}{\sum_{i=1}^{d}\sigma_i(\Phi)} \geq 1-\delta\right\}$, where $\{\sigma_i(\Phi)\}$ are the singular values of Φ in decreasing order, i.e., $\sigma_1 \geq \cdots \geq \sigma_d \geq 0$. Intuitively, the effective rank of a feature matrix represents the number of "effective" unique components that form the basis for linearly approximating the resulting Q-values. The calculation in Python is done as follows:

```
def compute_rank_from_features(feature_matrix, rank_delta=0.01):
    sing_values = np.linalg.svd(feature_matrix, compute_uv=False)
    cumsum = np.cumsum(sing_values)
    nuclear_norm = np.sum(sing_values)
    approximate_rank_threshold = 1.0 - rank_delta
    threshold_crossed = (cumsum >= approximate_rank_threshold * nuclear_norm)
    effective_rank = sing_values.shape[0] - np.sum(threshold_crossed) + 1
    return effective_rank
```

C Additional Experiments

C.1 Shallow and Deep Function Approximation

To further showcase the effect of activations on complex function approximation, we compare the single hidden layer Tanh (HR) network from Fig. 2 with a deep ReLU and Tanh network containing three hidden layers each. The comparison with shallow networks can be found in Fig. 13a and a comparison with deep networks can be found in Fig. 13b.

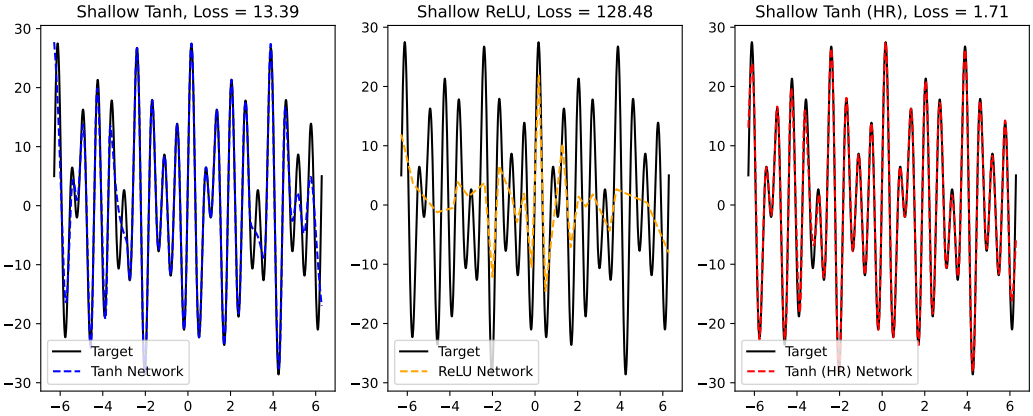

(a) Comparison of shallow networks for a nonlinear regression task. The Tanh and ReLU networks have a single hidden layer of 200 neurons, while the Tanh (HR) has a single hidden layer of 100 neurons but two preceding linear layers. The Tanh and ReLU networks have 601 parameters, while the Tanh (HR) network has 501 parameters. As found by Gulcehre et al. [2022], a shallow network activated by ReLU has a lower effective rank and consequently reduced network expressivity as compared to a Tanh activated network. Using a Hadamard representation, we achieve better function approximation while using less parameters.

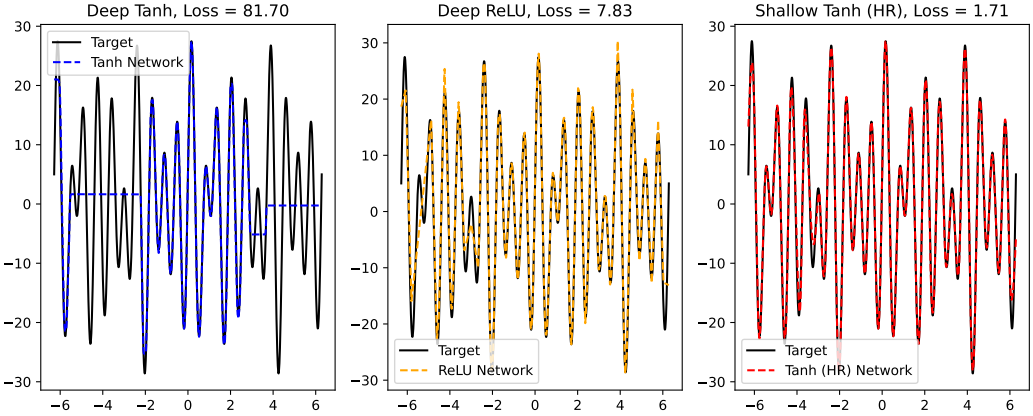

(b) Comparison of two deep networks and one shallow network for the same nonlinear regression task. The Tanh and ReLU networks have 3 hidden layers of 200 neurons each, while the Tanh (HR) network remains shallow. In line with common observations in deep learning, the ReLU activation thrives in deeper networks, in contrast to the Tanh activation. Interestingly, the shallow Tanh (HR) network still achieves better function approximation with only 0.6% of the deeper networks' parameters (81001 vs 501). No hyperparameter tuning or architecture search has been applied. Additional tests using deep Tanh (HR) networks gave similar function approximation as compared to the shallow Tanh (HR) network.

C.2 Increasing Representation Parameters

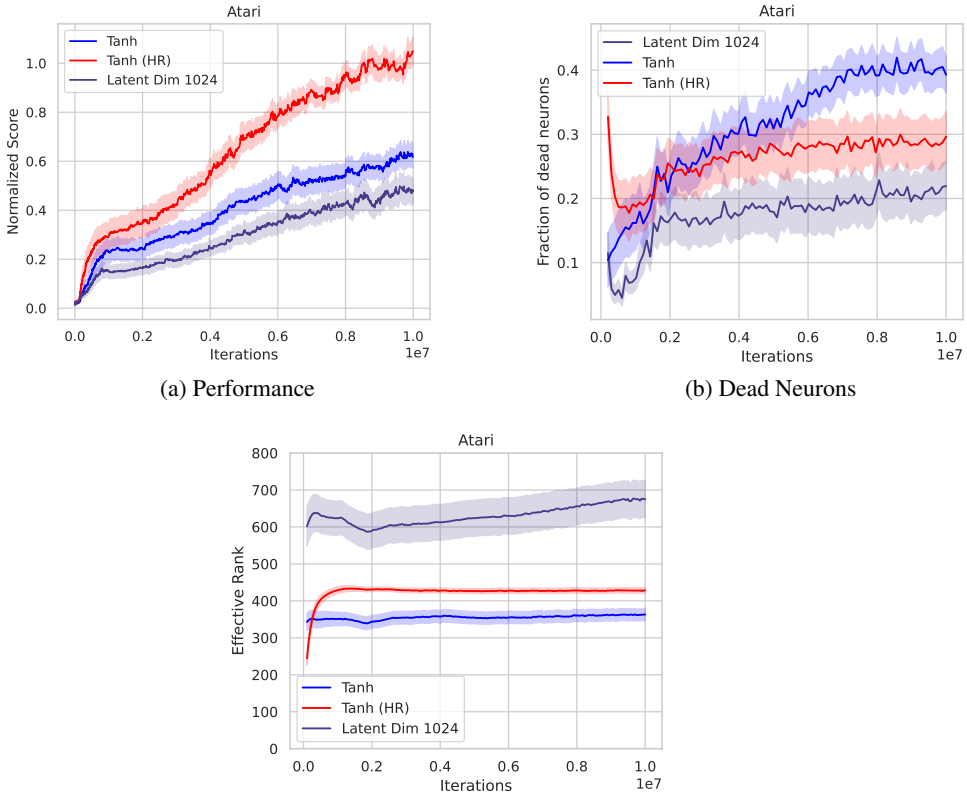

(a) Performance

(b) Dead Neurons

(c) Effective Rank

Figure 14: Comparison of a normal hyperbolic tangent (Tanh), a hyperbolic tangent with a higher representation dimension $z_t \in \mathbb{R}^{512 \to 1024}$ and a Hadamard representation using hyperbolic tangents. Comparisons are done on Performance (a), the fraction of dead neurons (b) and the effective rank of the representation z_t (c). Naturally, increasing the representation dimension z_t increases the effective rank of the representation, but using a larger representation dimension is not always preferable as it can negatively impact actual convergence.

C.3 Validating dying neuron probability derivations

As discussed in Section 3, the effect of using a Hadamard representation strongly depends on the activation function. These derivations are empirically validated by the results in Fig. 15. In practice, since a neural network prefers symmetry, a sigmoid saturates slightly faster to 0 than to 1. This could explain the very slight increase in dead neurons when using an HR with activations.

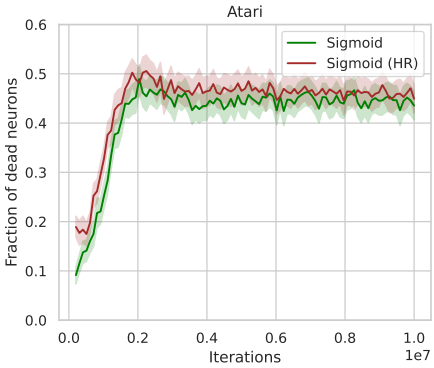

(a) Sigmoid with and without HR

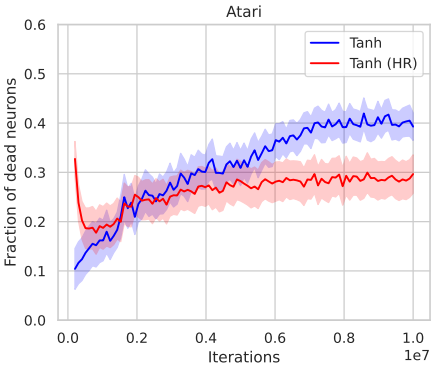

(b) Tanh with and without HR

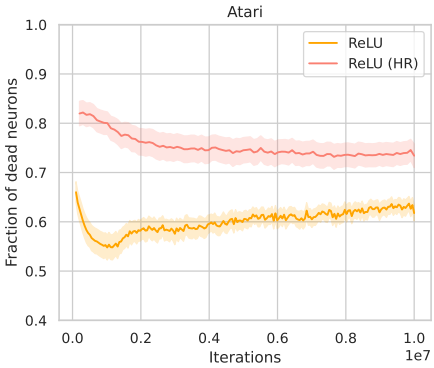

(c) ReLU with and without HR

Figure 15: By evaluating the effect of an HR on dying neurons through the lens of probability theory, we predicted that only the hyperbolic tangent benefits in this metric. Specifically, only a hyperbolic tangent was speculated to have a decrease in dying neurons. Using an HR with sigmoid activations would have no notable difference, and for an HR with ReLU activations an increase in dead neurons was expected. This empirically validates our hypotheses in Section 3.

C.4 ReLU activated Hadamard representation

Additional Atari experiments are provided comparing a ReLU activation with and without an HR. The normalized scores, dying neurons and the effective rank during training can be seen in fig. 16.

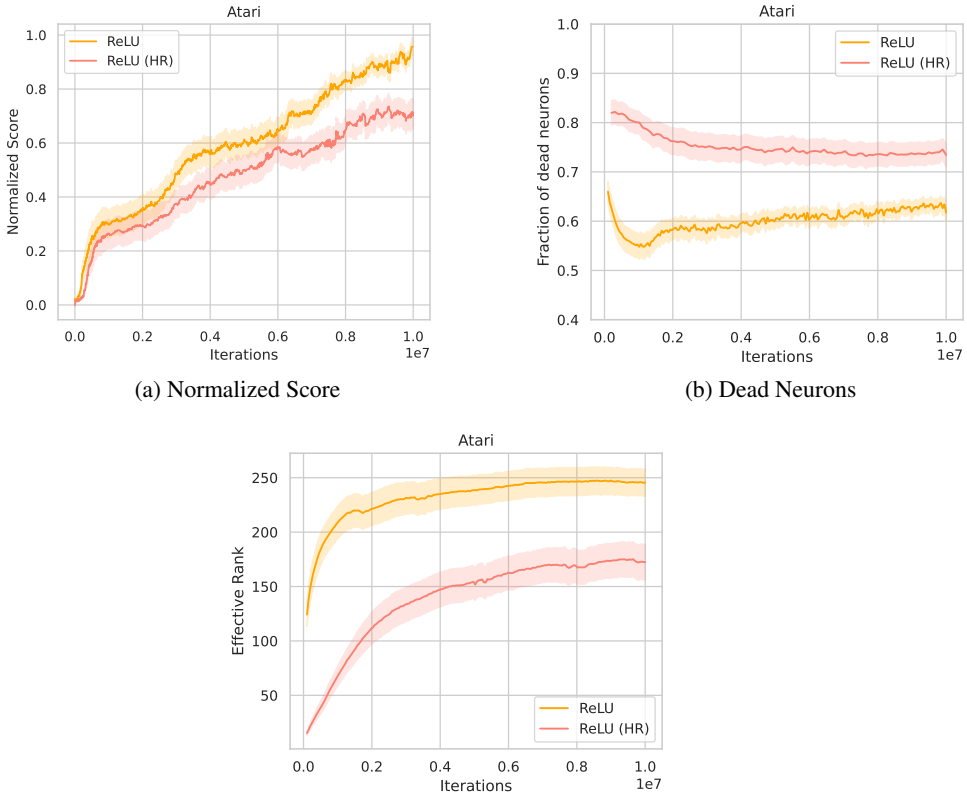

(a) Normalized Score

(b) Dead Neurons

(c) Effective Rank

Figure 16: As a Rectified Linear Unit creates sparse representations, it does not benefit from using an HR, since the final representation will consist of the Hadamard product between two sparse representations. Therefore, a decrease in both performance and effective rank and an increase in dead neurons can be expected.

D Atari

D.1 Evaluation Details

We normalize performance with respect to the ReLU baseline in `cleanrl` Huang et al. [2022]. The minimum and maximum score of the ReLU baseline are taken for each environment, and the normalized score for each environment is calculated as follows:

$$\text{Normalized Score} = \frac{\text{Score} - \text{Min Score}}{\text{Max Score} - \text{Min Score}} \tag{6}$$

where *Score* refers to the raw performance score of the model being evaluated, *Min Score* is a single value representing the lowest score obtained by the ReLU baseline (usually equivalent to random policy or even slightly worse), and *Max Score* is a single value representing the highest score achieved by the ReLU baseline in the same environment. To average, we sum the normalized scores for every run and take the mean.

The more official Human-Normalized Score, as referenced in Mnih et al. [2015], is calculated similarly but using human and random performance benchmarks:

$$\text{Human-Normalized Score} = \frac{\text{Score} - \text{Random Score}}{\text{Human Score} - \text{Random Score}} \tag{7}$$

where *Human Score* and *Random Score* refer to the scores recorded by human players and random agents, respectively. Calculating our performance according to the Human-Normalized Score leads to the plot seen in Fig. 17. Due to taking a subset of the full atari domain, the VideoPinball environment is extremely dominant in the Human-Normalized Score calculation. For a more realistic comparison of the methods, we therefore decided to use baseline-normalized scores in the main paper.

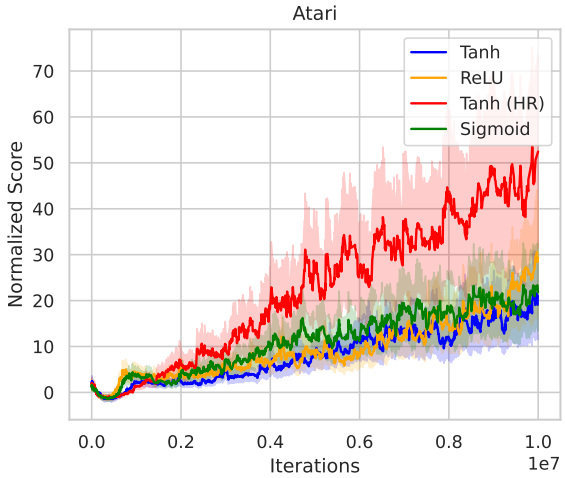

Figure 17: Human-Normalized performance (in multiples) with the standard deviation over the means in the Atari domain for 10M iterations (40M Frames).

D.2 Individual Environments

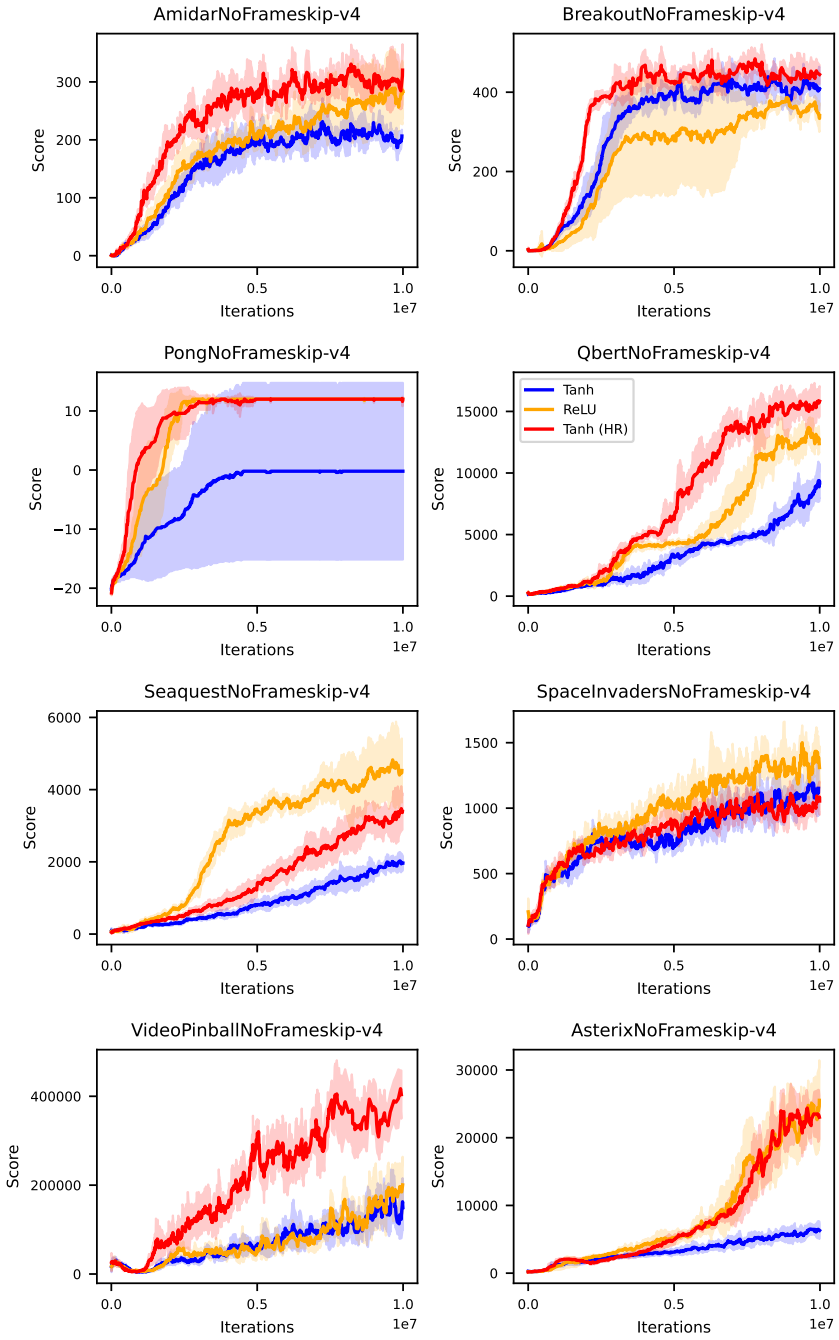

Figure 18: DQN Performance comparison on the individual Atari Environments. Plotted lines represent the mean taken over 5 seeds, with the standard deviations expressed as the shaded region. Eight popular Atari games in the RL community that are non-exploration driven were chosen due to computational limitations. No other games were tested.

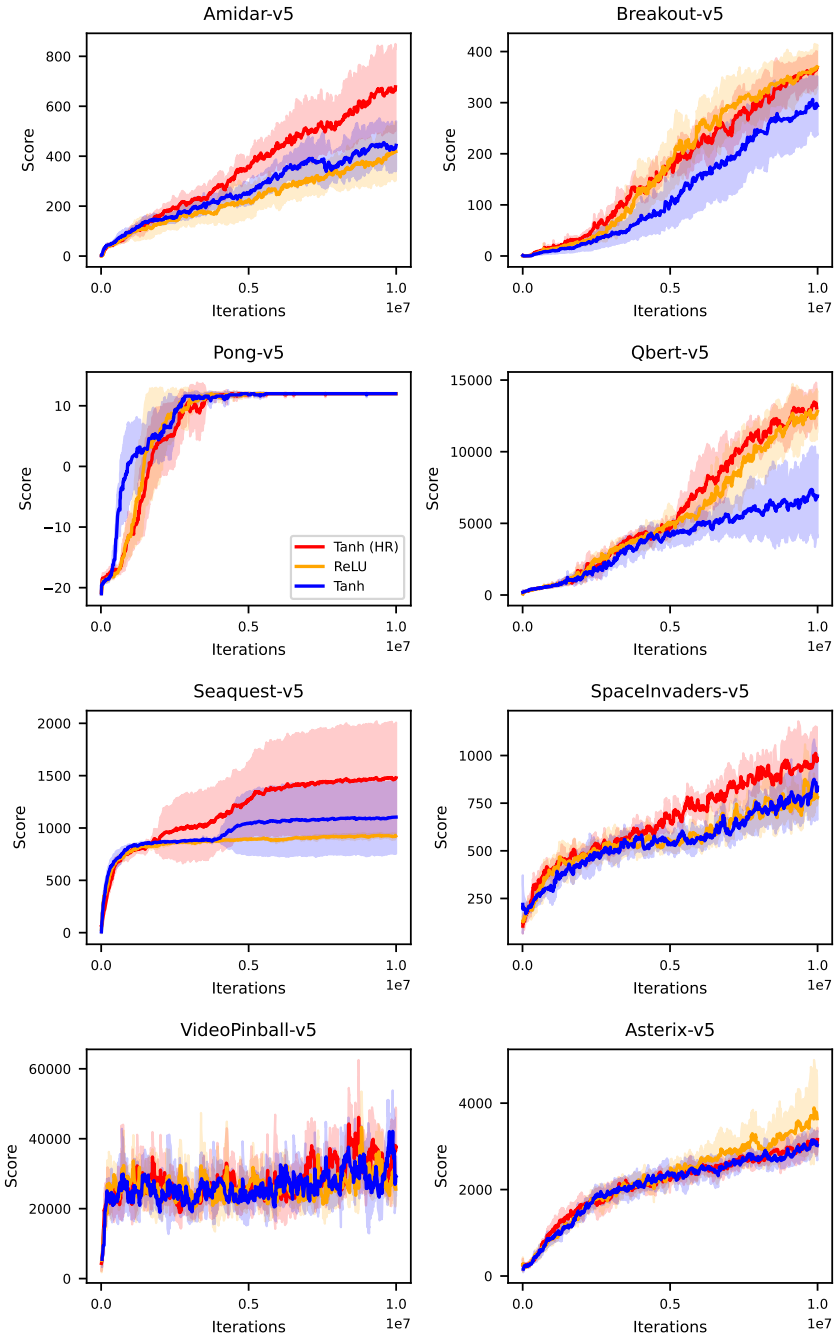

Figure 19: PPO Performance comparison on the individual Atari Environments. Plotted lines represent the mean taken over 5 seeds, with the standard deviations expressed as the shaded region. Eight popular Atari games in the RL community that are non-exploration driven were chosen due to computational limitations. No other games were tested.